

# Attractive photons in a quantum nonlinear medium

Ofer Firstenberg<sup>1\*</sup>, Thibault Peyronel<sup>2\*</sup>, Qi-Yu Liang<sup>2</sup>, Alexey V. Gorshkov<sup>3†</sup>, Mikhail D. Lukin<sup>1</sup> & Vladan Vuletić<sup>2</sup>

**The fundamental properties of light derive from its constituent particles—massless quanta (photons) that do not interact with one another<sup>1</sup>. However, it has long been known that the realization of coherent interactions between individual photons, akin to those associated with conventional massive particles, could enable a wide variety of novel scientific and engineering applications<sup>2,3</sup>. Here we demonstrate a quantum nonlinear medium inside which individual photons travel as massive particles with strong mutual attraction, such that the propagation of photon pairs is dominated by a two-photon bound state<sup>4–7</sup>. We achieve this through dispersive coupling of light to strongly interacting atoms in highly excited Rydberg states. We measure the dynamical evolution of the two-photon wavefunction using time-resolved quantum state tomography, and demonstrate a conditional phase shift<sup>8</sup> exceeding one radian, resulting in polarization-entangled photon pairs. Particular applications of this technique include all-optical switching, deterministic photonic quantum logic and the generation of strongly correlated states of light<sup>9</sup>.**

Interactions between individual photons are being explored in cavity quantum electrodynamics, where a single, confined electromagnetic mode is coupled to an atomic system<sup>10–12</sup>. Our approach is to couple a light field propagating in a dispersive medium to highly excited atomic states with strong mutual interactions<sup>13,14</sup> (Rydberg states). Similar to previous studies of quantum nonlinearities involving Rydberg states that were based on dissipation<sup>15–19</sup> rather than dispersion<sup>20</sup>, we make use of electromagnetically induced transparency (EIT) to slow down the propagation of light<sup>21</sup> in a cold atomic gas. By operating in a dispersive regime away from the intermediate atomic resonance (Fig. 1b), where atomic absorption is low and only weakly nonlinear<sup>22</sup>, we realize a situation in which Rydberg-atom-mediated coherent interactions between individual photons dominate the propagation dynamics of weak light pulses. Previous theoretical studies have proposed various scenarios for inducing strong interactions between individual photons<sup>2,3,23</sup> and for creating bound states of a few quanta<sup>4,5,7,24</sup>, a feature generic to strongly interacting quantum field theories. The main result reported here is the experimental realization of a photonic system with strong attractive interactions, including evidence for a predicted two-photon bound state.

Our experiment (outlined in Fig. 1a) makes use of an ultracold rubidium gas loaded into a dipole trap, as described previously<sup>19</sup>. The probe light of interest is  $\sigma^+$ -polarized, coupling the ground state,  $|g\rangle$ , to the Rydberg state,  $|r\rangle$ , via an intermediate state,  $|e\rangle$ , of linewidth  $\Gamma/2\pi = 6.1$  MHz by means of a control field that is detuned by  $\Delta$  below the resonance frequency of the upper transition,  $|e\rangle \rightarrow |r\rangle$  (Fig. 1b). Under these conditions, for a very weak probe field with mean incident photon rate  $R_i = 0.5 \mu\text{s}^{-1}$ , EIT is established when the probe detuning matches that of the control field (see Fig. 1c, which shows the probe transmission and phase shift). However, the Rydberg medium is extremely nonlinear: a probe photon rate of  $R_i = 5 \mu\text{s}^{-1}$  saturates the medium as a result of the Rydberg blockade<sup>25</sup>, yielding a probe spectrum close to the bare two-level response. Given the measured system bandwidth of about  $5 \mu\text{s}^{-1}$ , this implies a substantial nonlinear response with average pulse energies corresponding to less than one photon per inverse

bandwidth. We perform our experiments on the two-photon resonance  $|g\rangle \rightarrow |r\rangle$ , where, for  $|\Delta| > \Gamma$ , the transmission is approximately independent of the probe photon rate for our experimental parameters, yielding a purely dispersive nonlinearity. The linear dispersion at this resonance corresponds to a reduced probe group velocity of typically  $v_g = 400 \text{ m s}^{-1}$ , and the group velocity dispersion endows the photons with an effective mass<sup>26</sup> of  $m \approx 1,000\hbar\omega/c^2$ , where  $\omega$  is the optical frequency,  $\hbar$  is Planck's constant divided by  $2\pi$  and  $c$  is the speed of light in vacuum.

To explore the quantum dynamics in the propagation of photon pairs, we measure time-dependent two-photon correlation functions of the transmitted light (Fig. 1a). To determine both the amplitude and the phase of the  $\sigma^+$ -polarized probe field, we prepare input coherent light in a linearly polarized state,  $|V\rangle = (|\sigma^+\rangle + |\sigma^-\rangle)/\sqrt{2}$ , where the  $\sigma^-$ -polarized component (which is approximately non-interacting owing to the 15-fold-smaller transition strength) serves as a phase reference. To analyse the properties of photon pairs, we measure two-photon correlation functions,  $g_{\alpha\beta}^{(2)}$ , in different polarization bases,  $\alpha$  and  $\beta$  (Supplementary Fig. 3). The component  $g_{++}^{(2)}$  directly gives the probability density of the  $\sigma^+$ -polarized interacting photon pairs. Figure 1d shows  $g_{++}^{(2)}$ , for a control detuning of  $\Delta/2\pi = 14$  MHz, as a function of the time separation,  $\tau = t_1 - t_2$ , between the photons detected at times  $t_1$  and  $t_2$ , converted into a relative distance,  $r$ , in the medium using the group velocity,  $v_g$ . A prominent feature is the cusp at  $r = v_g\tau = 0$ , which is characteristic of a predicted two-photon bound state<sup>5,7</sup>, as discussed below.

The measured  $g_{\alpha\beta}^{(2)}$  allow us to reconstruct the two-photon density matrix,  $\rho$ , using quantum state tomography and maximum-likelihood estimation<sup>27,28</sup>. From  $\rho$ , we define an interaction matrix,  $\tilde{\rho}$ , by factoring out the linear response, such that  $\tilde{\rho}$  directly quantifies the nonlinearity (Methods). The density matrix approach is necessary to account for decoherence and technical imperfections. The probability density of two interacting  $\sigma^+$  photons,  $g_{++}^{(2)} = \tilde{\rho}_{++++}$ , and the nonlinear phase,  $\phi = \arg[\tilde{\rho}_{+-,-}]$ , acquired by the  $\sigma^+\sigma^+$  pair relative to a non-interacting  $\sigma^-\sigma^-$  pair, are shown in Fig. 2a, b for  $\Delta/2\pi = 14$  MHz. The time dependence allows us to extract the nonlinear phase as a function of the photon–photon separation. Clearly visible is the bunching of photons, that is, an increased probability for photons to exit the medium simultaneously ( $t_1 \approx t_2$ ), and a substantial nonlinear two-photon phase shift of  $-0.5$  rad in that region. Figure 2c shows the intensity correlation in the dissipation-dominated antibunching regime<sup>19</sup> at  $\Delta = 0$  and in the dispersive regime at  $|\Delta| > \Gamma$ , where there is bunching. Figure 2d displays the nonlinear phase for two different detunings. The transition from the dissipative regime to the dispersive is summarized in Fig. 3a, b. In the dispersive regime, the nonlinear phase shift,  $\phi(\tau = 0)$ , can reach  $(-0.32 \pm 0.02)\pi$ , at a detuning  $\Delta/2\pi = 9$  MHz and a linear transmission of order 50%. The observed signals, particularly  $\phi$ , are asymmetrical under a sign change of  $\Delta$ .

The origin of the quantum nonlinearity underlying these observations is explained by the following simple model. The repulsive van der Waals interaction between two Rydberg atoms,  $V(r) = \hbar C_6/r^6$ , tunes

<sup>1</sup>Department of Physics, Harvard University, Cambridge, Massachusetts 02138, USA. <sup>2</sup>Department of Physics and Research Laboratory of Electronics, Massachusetts Institute of Technology, Cambridge, Massachusetts 02139, USA. <sup>3</sup>Institute for Quantum Information and Matter, California Institute of Technology, Pasadena, California 91125, USA. <sup>†</sup>Present address: Joint Quantum Institute, NIST/University of Maryland, College Park, Maryland 20742, USA.

\*These authors contributed equally to this work.

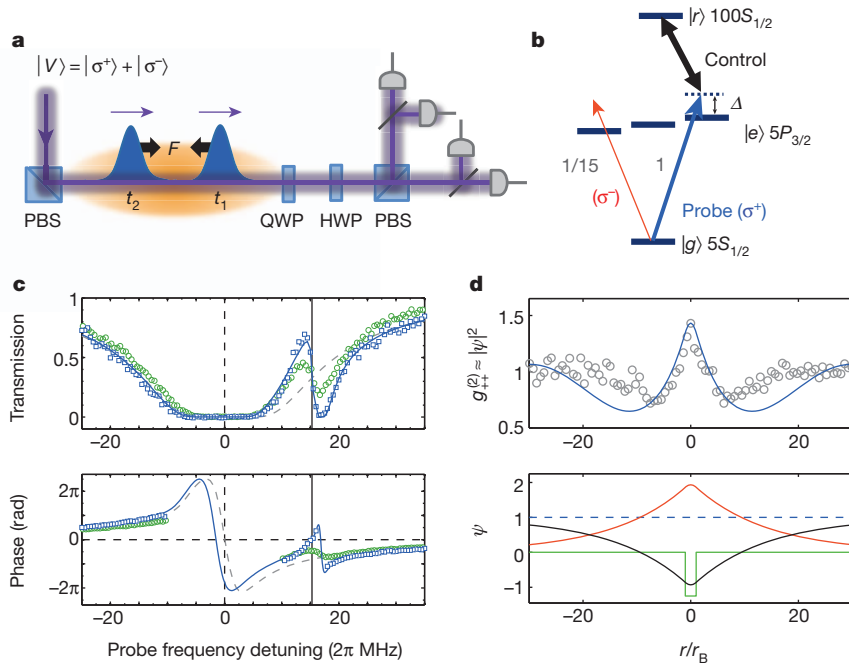


**Figure 1 | Photons with strong mutual attraction in a quantum nonlinear medium.** **a, b,** A linearly polarized weak laser beam near the transition  $|g\rangle \rightarrow |e\rangle$  at 780 nm is sent into a cold rubidium gas driven by a control laser near the transition  $|e\rangle \rightarrow |r\rangle$  at 479 nm. Strong nonlinear interactions between  $\sigma^+$ -polarized photons are detected using photon–photon correlation functions of the transmitted light for a set of different polarization bases, as determined by a quarter-wave plate (QWP), a half-wave plate (HWP) and a polarizing beam splitter (PBS). Here  $\sigma^-$  photons serve as a phase reference. **c,** Transmission spectra (top) and phase shift (bottom) for  $\sigma^+$  photons with an incoming rate of  $R_i = 0.5 \mu\text{s}^{-1}$  (blue squares) or  $R_i = 5 \mu\text{s}^{-1}$  (green circles), for a control field red-detuned by  $\Delta/2\pi = 15$  MHz. The blue line shows the theoretical spectrum. The spectrum at high probe rate approaches that of the undriven two-level

system (dashed grey; see also Supplementary Fig. 2). The solid vertical line corresponds to the EIT resonance. **d,** Photon bunching and two-photon bound state. Theoretically predicted photon–photon correlation function in the Schrödinger equation approximation (top, blue line) for  $\Delta/2\pi = 14$  MHz, with a potential well of width  $2r_B$  (bottom, green line). The bound state (bottom, red) and the superposition of scattering states (bottom, black) form the initial wavefunction,  $\psi = 1$  (bottom, dashed blue). The two-photon bound state results in the observed bunching in the correlation function,  $g_{++}^{(2)} \approx |\psi|^2$  (top, grey circles), where time has been converted into distance using the group velocity,  $v_g$ . The boundary effects resulting from the finite extent of the atom cloud become important for  $|r| \geq 5r_B$ .

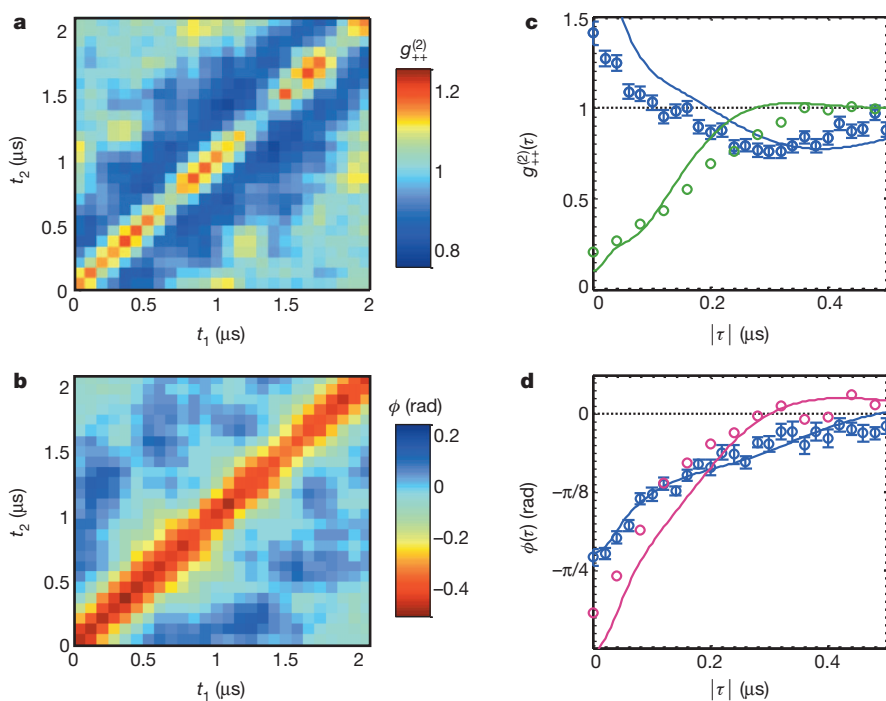


**Figure 2 | Propagation of interacting photon pairs.** **a, b,** Measured second-order correlation function (**a**) and nonlinear phase shift (**b**) of interacting photon pairs at  $\Delta = 2.3T$ . The photons are detected at times  $t_1$  and  $t_2$ . **c,** Second-order correlation function displayed as a function of the time difference,  $|\tau| = |t_1 - t_2|$ , between the photons, showing the transition from antibunching on resonance ( $\Delta = 0$ , green) to bunching at large detuning ( $\Delta = 2.3T$ , blue). Points are experimental data; lines are full numerical simulations. All  $g_{++}^{(2)}$  measurements are rescaled by their value at  $\tau > 1.5 \mu\text{s}$  (Supplementary Information). **d,** Nonlinear phase shift versus  $|\tau|$  for two different detunings ( $\Delta = 1.5T$ , purple, and  $\Delta = 2.3T$ , blue). The 1 s.d. error is  $\pm 30$  mrad, dominated by photon shot-noise.

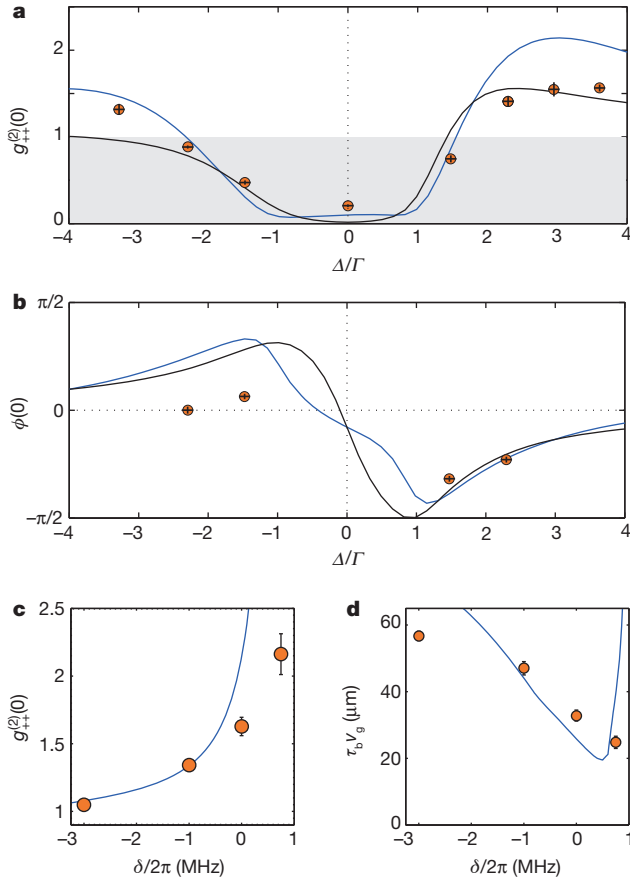


**Figure 3 | Dependence of the photon–photon interaction on detuning.** **a, b**, Equal-time two-photon correlation,  $g_{++}^{(2)}(0)$  (**a**), and nonlinear phase,  $\phi(0)$  (**b**), versus detuning,  $\Delta$ , from the intermediate state,  $|e\rangle$ . Blue lines are full theoretical simulations and black lines are the result of the Schrödinger equation approximation, assuming a simplified  $\delta$ -function potential. Vertical error bars represent 1 s.d. and horizontal error bars are  $\pm 0.5 \times 2\pi$  MHz. **c, d**, Equal-time correlation function (**c**) and spatial extent of the bunching feature (**d**) versus Raman detuning,  $\delta$ , from the EIT resonance  $|g\rangle \rightarrow |r\rangle$  for  $\Delta = 3\Gamma$ , showing increased photon–photon attraction due to a deeper potential near Raman resonance. The characteristic bunching timescale,  $\tau_b$ , is the half-width of the cusp feature of  $g_{++}^{(2)}$ , defined at half-height between the peak value at  $\tau = 0$  and the local minimum closest to  $\tau = 0$ . Error bars, 1 s.d. The theoretical model (solid line) breaks down close to the Raman resonance at  $\delta = 1.3 \times 2\pi \text{ MHz} \approx \Omega_c^2/4\Delta$ , where the single-photon component of the probe field is strongly absorbed.

the doubly excited Rydberg state far off EIT resonance for distances  $|r| < r_B$ , where  $r_B = \sqrt[6]{C_6/\gamma}$  is the Rydberg blockade radius<sup>14,29,30</sup>,  $C_6$  is the van der Waals coefficient,  $\gamma = \Omega_c^2/|4\Delta|$  is the EIT linewidth at detuning  $|\Delta| \gg \Gamma$  and  $\Omega_c$  is the Rabi frequency of the control field. Although the phase shift that would originate from the bare  $|g\rangle \rightarrow |e\rangle$  probe transition is suppressed by EIT for photons with large separation in the medium ( $|r| > r_B$ ), the light acquires this phase shift for small photon separations ( $|r| \leq r_B$ ) (Fig. 1c). This explicit dependence of the refractive index on photon–photon separation can be modelled in one dimension as a potential well with a characteristic width of  $2r_B$ . Qualitatively, a substantial two-photon phase shift arises for  $(r_B/l_a)(\Gamma/|\Delta|) \gtrsim 1$ , where  $l_a$  is the resonant attenuation length in the medium, that is, for sufficiently high atomic density. Furthermore, the probe field must also be compressed in the transverse direction to a waist size  $w < r_B$  to ensure that interactions occur. Using the Rydberg state  $100S_{1/2}$ , and for  $\Omega_c/2\pi = 10$  MHz, we obtain  $r_B \approx 18 \mu\text{m}$  at detunings of a few  $\Gamma$ ,  $l_a = 4 \mu\text{m}$  at the peak density, and  $w = 4.5 \mu\text{m}$ , fulfilling the conditions for strong interactions for  $|\Delta| \lesssim 5\Gamma$ .

The propagation of  $\sigma^+$ -polarized photon pairs in such a medium can be understood by first considering an idealized situation with no decoherence between the Rydberg state and the ground state. Then the steady state in a one-dimensional homogenous medium can be described by a two-photon wavefunction,  $\psi(z_1, z_2)$ , whose evolution is approximately governed by a simple equation<sup>19</sup> in terms of the centre-of-mass coordinate,  $R = (z_1 + z_2)/2$ , and the relative coordinate,  $r = z_1 - z_2$ :

$$i \frac{\partial \psi}{\partial R} = 4l_a \left[ i + \frac{2\Delta}{\Gamma} - \mathcal{V}(r) \frac{\Omega_c^2}{\Gamma^2} \right] \frac{\partial^2 \psi}{\partial r^2} + \frac{\mathcal{V}(r)}{l_a} \psi \quad (1)$$

Here the effective potential,  $\mathcal{V}(r) = [i + 2(\Delta/\Gamma)(1 + 2r^6/r_B^6)]^{-1}$ , approaches  $(i + 2\Delta/\Gamma)^{-1}$  inside the blockaded volume ( $|r| < r_B$ ) and approaches zero outside. The solution relates approximately to our measurements in the time domain for small  $|\tau|$  via  $\psi(R=L, r=v_g\tau) \approx \sqrt{g_{++}^{(2)}(\tau)} e^{i\phi(\tau)}$  (see Supplementary Information for the exact relation). Far off resonance ( $|\Delta| \gg \Gamma, \Omega_c$ ), equation (1) corresponds to a Schrödinger equation with  $R$  playing the part of effective time. The photons' effective mass,  $m \propto -\Gamma/16l_a\Delta$ , can be positive or negative depending on the sign of the detuning,  $\Delta$ . Because the sign of the potential also changes with  $\Delta$  (potential well for  $\Delta < 0$ ; barrier for  $\Delta > 0$ ), the effective force ( $F$  in Fig. 1a) in both cases is attractive and the resulting dynamics similar (Supplementary Information). However, the potential for  $\Delta < 0$  also has additional features near the edges of the well, corresponding to a Raman resonance  $|g\rangle \rightarrow |r\rangle$  for the interaction-shifted Rydberg state at some interatomic distance near  $|r| = r_B$ . These features are probably responsible for the deviation from symmetry (or antisymmetry) under the change of the sign of  $\Delta$  displayed in Fig. 3a, b.

In the experimentally relevant regime, the effective potential supports only one bound-state,  $\psi_B(r)$  (Fig. 1d). The initial wavefunction,  $\psi(R=0, r)=1$ , is a superposition of  $\psi_B(r)$  and the continuum of scattering states. The accumulation of probability near  $r=0$  can then be understood as arising from the interference between the bound and scattering states that evolve at different frequencies, and the observed bunching feature in  $g_{++}^{(2)}$  reveals the wavefunction of the two-photon bound state (Supplementary Information). As shown in Fig. 3a, b, the solution of the Schrödinger-like equation (1) with a simplified  $\delta$ -function potential captures the essential features of the nonlinear two-photon propagation. Additional experimental evidence for the bound-state dynamics is obtained by tuning the probe field relative to the EIT resonance, thereby varying the strength of the two-photon interaction potential. As the probe detuning approaches the Raman resonance, the difference in refractive indices inside and outside the blockade radius increases and the potential deepens (Supplementary Information and Fig. 1c). Consequently, the bound state becomes more localized and the bunching, quantified by  $g_{++}^{(2)}(0)$ , is enhanced (Fig. 3c, d). We note that the size of the two-photon bound state and, correspondingly, the width of the bunching feature,  $2\tau_b v_g \approx 70 \mu\text{m}$ , exceed the width of the potential well,  $2r_B \approx 35 \mu\text{m}$ , as expected for a potential with one weakly bound state.

Figures 2 and 3 also show the results of our full theoretical model, in which we numerically solve the set of propagation equations for the light field and atomic coherences. The model incorporates the longitudinal atomic density distribution and the decoherence of the Rydberg state (Supplementary Information). These simulations are in good agreement with our experimental results and the predictions of the simplified model (equation (1)), confirming that the evolution of the two-photon wave packet is dominated by the attractive force between the photons.

Finally, we study the quantum coherence and polarization properties of the transmitted photon pairs. In Fig. 4a, we compare the purity of the two-photon density matrix,  $\rho(\tau)$ , which includes photon interactions, with the purity of the product of one-photon matrices,  $\rho^{(1)} \otimes \rho^{(1)}$ , for non-interacting photons. At large photon separation,  $\tau$ , the purity,  $P(\tau)$ , of the two-photon density matrix is dominated by

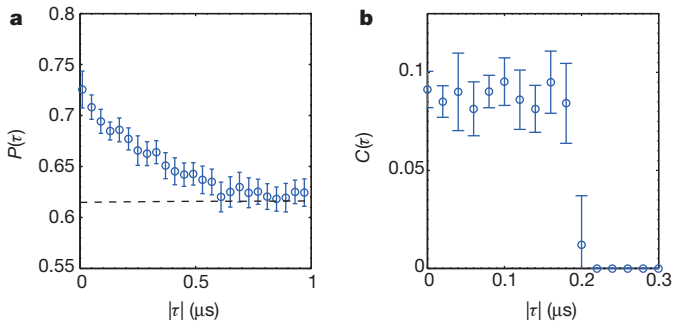


**Figure 4 | Quantum coherence and entanglement.** **a**, Purity,  $P(\tau) = \text{Tr}[\rho(\tau)^2]$ , of the measured two-photon density matrix,  $\rho$ , for  $\Delta = 2.3T$  (blue symbols), which at large photon separation approaches the purity expected from the measured one-photon density matrix,  $\text{Tr}[\rho^{(1)} \otimes \rho^{(1)}]^2$  (dotted black line). Interacting  $\sigma^+ \sigma^+$  photon pairs near  $\tau = 0$  exhibit lower decoherence. Error bars (1 s.d.) are derived from the uncertainty in the density matrix due to detection shot-noise. **b**, Concurrence,  $C(\tau)$ , calculated from  $\rho$ , indicating polarization entanglement of proximal photons on transmission through the quantum nonlinear medium.

the one-photon decoherence due to partial depolarization of the transmitted light (Supplementary Information). This depolarization is attributed to the difference in group delay,  $\tau_d$ , between the  $\sigma^+$  photons and the faster  $\sigma^-$  photons ( $\tau_d^+ - \tau_d^- = 280$  ns), which is not negligible compared with the coherence time of the probe laser (650 ns). At the same time,  $\sigma^+$  photons bound to each other travel faster and are more robust against this decoherence mechanism, as evidenced by the greater purity at small  $\tau$ . Even in the presence of this depolarization, the coherent nonlinear interaction in the dispersive medium produces entanglement in the outgoing polarization state of two photons. We quantify the degree of polarization entanglement in terms of a time-dependent concurrence,  $C(\tau)$  (Fig. 4b and Supplementary Information). The obtained value  $C(0) = 0.09 \pm 0.03$  indicates deterministic entanglement of previously independent photons on passage through the quantum nonlinear medium. The measured value is in reasonable agreement with the theoretical prediction,  $C_{\text{th}}(0) = 0.13$ , calculated for a conditional phase  $\phi(0) = \pi/4$ , purity  $P(0) = 0.73$  and 50%  $\sigma^+$  linear transmission.

In our experiment, the transmission and achievable nonlinear phase are limited by the laser linewidth, the atomic motion and the available control-field intensity. These technical limitations can be circumvented by using stronger control lasers with improved frequency stability and colder atomic clouds trapped in both the ground state and the Rydberg state. Although in our present system the nonlinear phase would not be uniformly acquired by a bandwidth-limited two-photon pulse, a high-fidelity two-photon phase gate may be achievable using, for example, a counter-propagating geometry and greater optical depths<sup>14</sup>.

The realization of coherent, dispersive photon–photon interactions opens several new research directions. These include the exploration of a novel quantum matter composed from strongly interacting, massive photons<sup>9</sup>. Measurements of higher-order correlation functions may give direct experimental access to quantum solitons composed of a few interacting bosons<sup>24</sup>, or to the detection of crystalline states of a photonic gas<sup>9</sup>. By colliding two counter-propagating photons, it may be possible to imprint a spatially homogeneous phase shift of  $\pi$  on the photon pair, corresponding to a deterministic quantum gate<sup>14</sup> for scalable optical quantum computation<sup>13</sup>. Finally, by accessing other Rydberg states via, for example, microwave transitions, it may become possible to control the state of multiphoton pulses with just one quantum of light, thereby realizing a single-photon transistor<sup>6,31</sup> for applications in quantum networks, and the creation of multiphoton entangled states.

## METHODS SUMMARY

The experimental setup is detailed in ref. 19. The average resonant optical depth along the atomic cloud is 22, and the peak atomic density is  $10^{12} \text{ cm}^{-3}$ .

Probe pulses at an average photon rate of  $1.6 \mu\text{s}^{-1}$  are sent into the cell during the 5.5- $\mu\text{s}$  dark-time periods of a modulated optical trap. For the quantum state tomography, we measure the photon coincidence rates in six polarization bases,  $\{q, h\} = \{\pi/4, \pi/4\}, \{0, 0\}, \{\pi/8, \pi/8\}, \{0, \pi/16\}, \{\pi/8, \pi/16\}$  and  $\{\pi/8, 0\}$ , where  $q$  and  $h$  are the angles of the quarter- and half-wave plates. The duration of the coincidence time bins, varying between 20 and 80 ns, is chosen to capture the temporal dynamics of the correlation functions with reasonable signal-to-noise ratio. For each  $(t_1, t_2)$  time bin, we numerically optimize a Hermitian, positive-semidefinite two-photon density matrix,  $\rho(t_1, t_2)$ , and one-photon density matrix,  $\rho^{(1)}(t)$ . To extract the nonlinear phase from  $\rho(t_1, t_2)$ , we rescale for the linear dispersion and loss effects by defining the interaction matrix  $\tilde{\rho}_{ij}(t_1, t_2) = \rho_{ij}(t_1, t_2) / [\rho^{(1)}(t_1) \otimes \rho^{(1)}(t_2)]_{ij}$  in the circular-polarization basis. The interaction matrix generalizes the standard  $g_{\alpha, \beta}$  definition to account for nonlinear phases and decoherence, and all its elements are equal to 1 in the absence of nonlinearity.

**Online Content** Any additional Methods, Extended Data display items and Source Data are available in the online version of the paper; references unique to these sections appear only in the online paper.

Received 28 May; accepted 29 July 2013.

Published online 25 September 2013.

1. Scully, M. O. & Zubairy, M. S. *Quantum Optics* (Cambridge Univ. Press, 1997).
2. Milburn, G. J. Quantum optical Fredkin gate. *Phys. Rev. Lett.* **62**, 2124–2127 (1989).
3. Imamoglu, A. Schmidt, H. Woods, G. & Deutsch, M. Strongly interacting photons in a nonlinear cavity. *Phys. Rev. Lett.* **79**, 1467–1470 (1997).
4. Deutsch, I. H., Chiao, R. Y. & Garrison, J. C. Diphotons in a nonlinear Fabry-Pérot resonator: bound states of interacting photons in an optical “quantum wire”. *Phys. Rev. Lett.* **69**, 3627–3630 (1992).
5. Shen, J.-T. & Fan, S. Strongly correlated two-photon transport in a one-dimensional waveguide coupled to a two-level system. *Phys. Rev. Lett.* **98**, 153003 (2007).
6. Chang, D. E., Sørensen, A. S., Demler, E. A. & Lukin, M. D. A single-photon transistor using nanoscale surface plasmons. *Nature Phys.* **3**, 807–812 (2007).
7. Cheng, Z. & Kurizki, G. Optical “multiexcitons”: quantum gap solitons in nonlinear Bragg reflectors. *Phys. Rev. Lett.* **75**, 3430–3433 (1995).
8. Turchette, Q. A., Hood, C., Lange, W., Mabuchi, H. & Kimble, H. Measurement of conditional phase shifts for quantum logic. *Phys. Rev. Lett.* **75**, 4710–4713 (1995).
9. Chang, D. E. *et al.* Crystallization of strongly interacting photons in a nonlinear optical fibre. *Nature Phys.* **4**, 884–889 (2008).
10. Fushman, I. *et al.* Controlled phase shifts with a single quantum dot. *Science* **320**, 769–772 (2008).
11. Rauschenbeutel, A. *et al.* Coherent operation of a tunable quantum phase gate in cavity QED. *Phys. Rev. Lett.* **83**, 5166–5169 (1999).
12. Kirchmair, G. *et al.* Observation of quantum state collapse and revival due to the single-photon Kerr effect. *Nature* **495**, 205–209 (2013).
13. Saffman, M., Walker, T. G. & Mølmer, K. Quantum information with Rydberg atoms. *Rev. Mod. Phys.* **82**, 2313–2363 (2010).
14. Gorshkov, A. V., Otterbach, J., Fleischhauer, M., Pohl, T. & Lukin, M. D. Photon-photon interactions via Rydberg blockade. *Phys. Rev. Lett.* **107**, 133602 (2011).
15. Pritchard, J. D. *et al.* Cooperative atom-light interaction in a blockaded Rydberg ensemble. *Phys. Rev. Lett.* **105**, 193603 (2010).
16. Maxwell, D. *et al.* Storage and control of optical photons using Rydberg polaritons. *Phys. Rev. Lett.* **110**, 103001 (2013).
17. Dudin, Y. O. & Kuzmich, A. Strongly interacting Rydberg excitations of a cold atomic gas. *Science* **336**, 887–889 (2012).
18. Petrosyan, D., Otterbach, J. & Fleischhauer, M. Electromagnetically induced transparency with Rydberg atoms. *Phys. Rev. Lett.* **107**, 213601 (2011).
19. Peyronel, T. *et al.* Quantum nonlinear optics with single photons enabled by strongly interacting atoms. *Nature* **488**, 57–60 (2012).
20. Parigi, V. *et al.* Observation and measurement of interaction-induced dispersive optical nonlinearities in an ensemble of cold Rydberg atoms. *Phys. Rev. Lett.* **109**, 233602 (2012).
21. Kasapi, A., Jain, M., Yin, G. Y. & Harris, S. E. Electromagnetically induced transparency: propagation dynamics. *Phys. Rev. Lett.* **74**, 2447–2450 (1995).
22. Venkataraman, V., Saha, K. & Gaeta, A. L. Phase modulation at the few-photon level for weak-nonlinearity-based quantum computing. *Nature Photon.* **7**, 138–141 (2012).
23. Rajapakse, R. M., Bragdon, T., Rey, A. M., Calarco, T. & Yelin, S. F. Single-photon nonlinearities using arrays of cold polar molecules. *Phys. Rev. A* **80**, 013810 (2009).
24. Drummond, P. D. & He, H. Optical mesons. *Phys. Rev. A* **56**, R1107–R1109 (1997).
25. Lukin, M. D. *et al.* Dipole blockade and quantum information processing in mesoscopic atomic ensembles. *Phys. Rev. Lett.* **87**, 037901 (2001).
26. Fleischhauer, M., Imamoglu, A. & Marangos, J. P. Electromagnetically induced transparency: optics in coherent media. *Rev. Mod. Phys.* **77**, 633–673 (2005).

27. James, D. F. V., Kwiat, P. G., Munro, W. J. & White, A. G. Measurement of qubits. *Phys. Rev. A* **64**, 052312 (2001).
28. Adamson, R. B. A., Shalm, L. K., Mitchell, M. W. & Steinberg, A. M. Multiparticle state tomography: hidden differences. *Phys. Rev. Lett.* **98**, 043601 (2007).
29. Sevinçli, S., Henkel, N., Ates, C. & Pohl, T. Nonlocal nonlinear optics in cold Rydberg gases. *Phys. Rev. Lett.* **107**, 153001 (2011).
30. Heidemann, R. *et al.* Evidence for coherent collective Rydberg excitation in the strong blockade regime. *Phys. Rev. Lett.* **99**, 163601 (2007).
31. Chen, W. *et al.* All-optical switch and transistor gated by one stored photon. *Science* **341**, 768–770 (2013).

**Supplementary Information** is available in the online version of the paper.

**Acknowledgements** We thank H. P. Büchler, T. Pohl, J. Otterbach, P. Strack, M. Gullans and S. Choi for discussions. This work was supported by the NSF, the CUA, DARPA and

the AFOSR Quantum Memories MURI and the Packard Foundations. O.F. acknowledges support from the HQOC. A.V.G. and M.D.L. thank KITP for hospitality. A.V.G. acknowledges funding from the Lee A. DuBridge Foundation and the IQIM, an NSF Physics Frontiers Center with support of the Gordon and Betty Moore Foundation.

**Author Contributions** The experiment and analysis were carried out by O.F., T.P. and Q.-Y.L. The theoretical modelling was done by A.V.G. All experimental and theoretical work was supervised by M.D.L. and V.V. All authors discussed the results and contributed to the manuscript.

**Author Information** Reprints and permissions information is available at [www.nature.com/reprints](http://www.nature.com/reprints). The authors declare no competing financial interests. Readers are welcome to comment on the online version of the paper. Correspondence and requests for materials should be addressed to M.D.L. ([lukin@fas.harvard.edu](mailto:lukin@fas.harvard.edu)) or V.V. ([vuletic@mit.edu](mailto:vuletic@mit.edu)).

## METHODS

The experimental setup is detailed in ref. 19, with the following modifications. The dipole trap is periodically switched off with a 5.5- $\mu\text{s}$  half-period, and the measurements are performed during the dark time to avoid inhomogeneous broadening. Photons detected in the first 1.5  $\mu\text{s}$  after the dipole trap is turned off are not included in the analysis, to guarantee steady-state EIT. For each experimental cycle, data are accumulated over 400 periods of the dipole-trap modulation. The trapped atomic cloud has a longitudinal root mean squared length of  $\sigma_{\text{ax}} = 36 \mu\text{m}$  and a peak atomic density of  $\rho_0 = 10^{12} \text{cm}^{-3}$ . The average resonant optical depth is 22, with less than 20% variation over the measurement time. The probe and control beams are counter-propagating to reduce the residual Doppler broadening to  $50 \times 2\pi \text{kHz}$ . Linearly polarized probe laser light enters the medium at an average photon rate of  $1.6 \mu\text{s}^{-1}$ . Quarter- and half-wave plates at angles  $q$  and  $h$ , respectively, followed by a polarizing beam splitter, project the outgoing probe light onto a chosen polarization basis (Fig. 1a). Four single-photon counting modules measure the pair correlation events at times  $t_1$  and  $t_2$ . Normalized second-order correlation functions,  $g_{\alpha\beta}^{(2)}$ , are calculated using the photon coincidence counts between the different detectors and the average count rates. The time bins (80 ns for  $g_{\alpha\beta}^{(2)}(t_1, t_2)$  and 20 or 40 ns for  $g_{\alpha\beta}^{(2)}(\tau)$ ) were chosen to capture the temporal dynamics of the correlation functions with reasonable signal-to-noise ratio.

In the quantum state tomography, we numerically optimize a Hermitian, positive-semidefinite two-photon density matrix

$$\rho = \begin{pmatrix} \rho_{++++} & \rho_{++s} & \rho_{++--} & 0 \\ \rho_{s+++} & \rho_{s,s} & \rho_{s--} & 0 \\ \rho_{--,+} & \rho_{--s} & \rho_{--} & 0 \\ 0 & 0 & 0 & \rho_{A,A} \end{pmatrix}$$

in the two-qubit basis  $\{|\sigma_1^+ \sigma_2^+\rangle, |S\rangle, |\sigma_1^- \sigma_2^-\rangle, |A\rangle\}$ , where  $|S\rangle = (|\sigma_1^+ \sigma_2^-\rangle + |\sigma_1^- \sigma_2^+\rangle)/\sqrt{2}$  and  $|A\rangle = (|\sigma_1^+ \sigma_2^-\rangle - |\sigma_1^- \sigma_2^+\rangle)/\sqrt{2}$ . Because the two photons have the same frequency and spatial mode, there is no coherence between the  $3 \times 3$  symmetric and  $1 \times 1$  antisymmetric subspaces<sup>28</sup>. We measure in six required polarization bases, chosen as  $\{q, h\} = \{\pi/4, \pi/4\}, \{0, 0\}, \{\pi/8, \pi/8\}, \{0, \pi/16\}, \{\pi/8, \pi/16\}$  and  $\{\pi/8, 0\}$ , to set the ten degrees of freedom in  $\rho(t_1, t_2)$ . The optimization follows the maximum-likelihood estimate<sup>27</sup>, where all coincidence measurements are considered. The one-photon density matrix,  $\rho^{(1)}(t)$ , is reconstructed using the same technique. To extract the nonlinear phase from  $\rho(t_1, t_2)$ , we rescale for the linear dispersion and loss effects by defining the interaction matrix  $\tilde{\rho}_{i,j}(t_1, t_2) = \rho_{i,j}(t_1, t_2) / [\rho^{(1)}(t_1) \otimes \rho^{(1)}(t_2)]_{i,j}$  in the basis  $\{|\sigma_1^+ \sigma_2^+\rangle, |\sigma_1^+ \sigma_2^-\rangle, |\sigma_1^- \sigma_2^+\rangle, |\sigma_1^- \sigma_2^-\rangle\}$ . The interaction matrix generalizes the standard definition of  $g^{(2)}$  to account for nonlinear phases and decoherence, and all its elements are equal to 1 in the absence of nonlinearity. In Supplementary Fig. 3, we compare the measured photon-photon correlation functions with those calculated from  $\tilde{\rho}$  (see also Supplementary Fig. 4). The colour maps in Fig. 2 presenting values derived from  $\rho(t_1, t_2)$  have been smoothed using an unweighted, nearest-neighbour, rectangular sliding average.